Journal of Chemical Health Risks

www.jchr.org

JCHR (2025) 15(4), 662-669 | ISSN:2251-6727

Efficient Fe^{2+} Ions Adsorption by Functionalized Reduced Graphene Oxide Derived from Pencil Lead

Soni Tyagi[1], Dr. Soumita Talukdar[1,2,*]

[1]*School of Engineering & Sciences, G.D. Goenka University, Gurugram, Haryana-122103, INDIA*

(Received: 16 May 2025 Revised: 20 June 2025 Accepted: 02 July 2025)

KEYWORDS

reduced Graphene Oxide (rGO), Adsorption, heavy metals

ABSTRACT:

Introduction: One of the environmental contaminants to which humans can become acutely and dangerously poisoned is heavy metal exposure through food and drink. Toxic heavy metals, whether from natural or artificial sources, such as $Pb^{2+,}$ $Cu^{2+,}$ Ag^{+}, and Zn^{2+}, etc. can contaminate water. It seems highly essential to remove toxic heavy metals from water effectively. Among these, adsorption exhibits a promising approach because of its affordability, efficiency, and reusability.

Objectives: Adsorbents based on graphene, graphene oxide (GO), and reduced GO (rGO) have garnered significant attention due to their efficaciousness in eliminating heavy metals from the environment. Excellent electrical, mechanical, optical, and transport capabilities have led to a variety of uses for graphene and its derivatives, including GO. An array of modified graphene and graphene oxide was reported to be extensively used for heavy metal adsorption. Furthermore, the use of graphene oxide-based nanocomposites as adsorbents for heavy metals is being studied extensively.

Methods: In this study, GO was synthesized from commercially available pencil lead, which was further reduced and functionalized with amine, thiol, and carboxyl groups using thiourea and mercaptoacetic acid to produce rGO. The functionalization was confirmed from Fourier Transform Infrared Spectroscopy (FTIR) and EDAX analysis, showcasing the presence of C=N, N-H, and S-H peaks.

Results: TEM and Raman spectroscopy analysis confirmed the formation of rGO sheets with characteristic D and G bands, also exhibited by XRD analysis. The as-synthesised rGO was further used for systematic adsorption of Fe^{2+} ions from aqueous solution.

Conclusions: The various adsorption isotherm was analysed, and the adsorption was found to be dominated by monolayer adsorption, undergoing both physisorption and chemisorption. The adsorption of Fe^{2+} ions by rGO follows pseudo-first order kinetics, with an optimum adsorption percentage to be approximately 89.69%.

1. Introduction

The world faces a serious issue with wastewater management and recovery due to the world's fast population growth and ongoing development. Industries that produce heavy metals and other stubborn organic pollutants, such as electroplating, mining, refineries, printing, dyeing, and tanning, release effluents into the environment. Significant amounts of heavy metals are released into the environment via additional sources, including urban runoff, municipal wastewater, landfill leachate, and agricultural practices (Rizzo et al., 2019). In contrast to organic contaminants, heavy metals are less biodegradable and remain stable in the environment, building up to dangerous levels in the soil, water, and food chain. Heavy metals can be adsorbed by living things because of their high solubility in aquatic environments, and they often build up in human bodies by attaching to proteins and nucleic acids. Even at low concentrations, heavy metal ions have been shown to have detrimental impacts on human health (Gupta et al., 2011). Human concerns include clotting, liver necrosis, cardiovascular collapse, gastrointestinal bleeding, respiratory disorders, severe anaemia, and gradual organ failure (Khorshidi et al., 2020). For example, the central nervous system, haematological, renal, gastrointestinal, cardiovascular, and reproductive systems may all be toxicologically affected by lead exposure (Mirnezami et al., 2019). Moreover, gastrointestinal, cardiovascular, and dermatological issues have all been connected to

Journal of Chemical Health Risks
www.jchr.org
JCHR (2025) 15(4), 662-669 | ISSN:2251-6727

long-term arsenic consumption (Hong et al., 2014). Consequently, strict regulations containing heavy metals have been placed on industrial effluents (Sherlala et al., 2018). Specifically, at extremely low concentrations, Fe(II) and Cu(II) are both nutrients involved in many biological functions, such as cofactors for enzyme activity, but at excessive quantities, they become poisonous. The permitted limits of Fe(II) and Cu(II) in drinking water are 2.0 $mg \cdot L^{-1}$ and 0.3 $mg \cdot L^{-1}$, respectively, according to WHO regulations (Hamdouni et al., 2016). Indeed, a high Fe(II) level in the water may serve as a substrate for the bacterial contamination that develops in the ducts (Akaji & Dewez, 2020a). Chronic exposure to Fe(II) has been linked to negative health outcomes, including decreased haematopoiesis. Furthermore, gastrointestinal, liver, or kidney problems, as well as keratinization, might be brought on by Cu(II) excess (Akaji & Dewez, 2020b).

Numerous adsorbent forms, including clay minerals, activated carbon, porous carbon, porous carbon that has been loaded with ZnO nanoparticles, and nanomaterials, have been developed to remove pollutants from the environment (Ratnam et al., 2023). Since graphene-based materials have favourable physicochemical properties-such as high specific surface area and adsorption capacity, mechanical strength, radiation resistance, and chemical stability over a wide pH range, they have emerged as an effective and promising adsorbent for the removal of heavy metals, including radionuclides(Li et al., 2012). The hydrophobic feature of graphene sheets is attributed to their hexagonal arrangement of sp^2 hybridized carbon atoms. Although graphene-based materials are said to be suitable for a variety of environmental applications, their hydrophobicity limits their use as an adsorbent for metal ion adsorption in aqueous media. Because of the addition of hydroxyls and epoxides in the basal layer and carbonyl and carboxyl groups at the plane edges, the modification of graphene to graphene oxide confers hydrophilic properties (Verma & Dutta, 2015). Because of π-π stacking and van der Waals interactions, GO is prone to irreversible aggregation and restacking, which primarily impacts its applications and overall performance. One possible way to prevent aggregation and build a composite with the features of both materials is to functionalize the surface of graphene oxide (GO) at the moment of reduction (Patel et al., 2023).

The primary goal of this study was to create graphene oxide and functionalize it with thioglycolic acid (mercapto acetic acid) and thiourea to give metals in solution a powerful adsorption capability, which supplies the functional groups COOH, SH, and NH_2 needed for efficient metal complexation. By complexing iron species with phenanthroline, the colorimetric approach is utilized in this study to determine the quantitative adsorption of Fe^{2+} ions. The adsorption process is extensively examined using adsorption kinetics and adsorption isotherm models, and the adsorption of Fe^{2+} ions on reduced graphene oxide functionalized with thiourea and thioglycolic acid is optimized.

2. Materials and Methods

2.1 Chemicals

Pencil of Nataraj company for graphite, concentrated sulphuric acid (H_2SO_4, 98%), H_3PO_4 ammonia (NH_3) of Rankem, India Pvt. Ltd. have been used. Sodium nitrate ($NaNO_3$) and Potassium permanganate ($KMnO_4$) of CDH, hydrogen peroxide(H_2O_2) of Loba Chemie Pvt. Ltd., arranged by G D Goenka University campus, have been used. Every reagent utilized in the synthesis was of laboratory quality and didn't require any additional purification.

2.2. Synthesis of modified graphene oxide

Hummer's approach was initially used to synthesize graphene oxide (GO) from graphite powder, with a few minor adjustments. Conc. H_2SO_4 (60 mL) and H_3PO_4 (7 mL) were combined, then chilled in an ice bath. 0.5 g of graphite powder, 1.5 g of $NaNO_3$, and 4.0 g of $KMnO_4$ were added to this solution. For two hours, the reaction mixture was magnetically stirred on an ice bath. After that solution was prepared on a magnetic stir for 2 h, keeping the temperature between 70-80°C, 10mL of H_2O_2 was added to this solution. A glossy, golden-brown substance was discovered.

2.2.1. Functionalisation of GO to rGO

50 mL of the as-synthesized modified GO solution was taken, 0.76 g of Thiourea and 0.76 mL of mercapto acetic acid were added, and then refluxed for 2 hours at 180 °C. The mixture was then subjected under centrifugation for 10 minutes at 3500 rpm to separate the solid material that had developed at this point. After drying, a thick, black precipitate was produced.

Journal of Chemical Health Risks
www.jchr.org
JCHR (2025) 15(4), 662-669 | ISSN:2251-6727

2.3 Characterization techniques

By employing a Nicolet, Nexus FT-IR spectrometer to record FT-IR spectra, the functional groups of GO and Thio_MAA@GO (rGO) were examined. Powder X-ray diffractometer (Bruker ARS D8 advanced) operating at 40 kV was used to do the XRD studies of GO and rGO. The radiation source was a graphite monochromatized Cu Kα with a wavelength of 1.54 ˚A, scanning at a scan rate of 2~ min^{-1} in a wide-angle region from 5° to 85° on the 2θ scale. An excitation energy of λ = 514 nm was used to record the Raman spectra of GO and rGO using a Raman microscope (Renishaw). A 200 kV FEI Technai-G2 transmission electron microscope (TEM) was used to study the morphology of the rGO. Drop casting rGO nanosheets was dispersed in deionised water onto a carbon-coated 150 mesh copper grid and allowed to dry at room temperature, producing the samples for TEM investigations.

2.4 Adsorption studies of Fe^{2+}

Using the spectrophotometric approach, the systematic adsorption of Fe^{2+} ions was determined by measuring the absorbance of the iron-phenanthroline complex, which shows a maximum at 510 nm. Using a Shimadzu UV-1800, the absorbance of the Fe^{2+} ion complexed with phenanthroline was measured at 510 nm. The absorbance of the complex was proportional to the Fe^{2+} ion concentration. Interference studies were done in the presence of various metal ions to evaluate the sensitivity of Thermodynamic studies were performed at different temperatures, and q_e is evaluated.

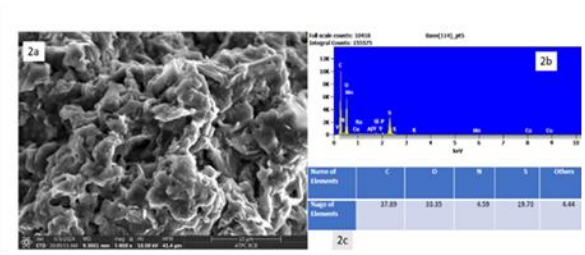

Figure 1 (a) SEM image of rGO, (b) EDAX spectra of rGO, (c) Atomic %of various elements in rGO

3. Result and Discussions

3.1. Characterization of Thio_MAA@GO (rGO)

The FTIR (Fig.1) spectra of the synthesized GO represent the existence of C–OH and alkoxy C–O vibrations by the adsorption peaks in the GO spectra at 1406 (Seenivasan et al., 2015) and 1036 cm^{-1}(Banazadeh et al., 2015). Following functionalisation with thio urea and mercaptoacetic acid, new distinctive peaks emerged as the C=N stretching peak was located at 1331 cm^{-1}, the N–H bending peak was observed at 1060 cm^{-1}, characteristic S–H bending peak was observed at 922 cm^{-1}(Kumar & Jiang, 2015), and the N–H wagging peak was located at 826 cm^{-1}.

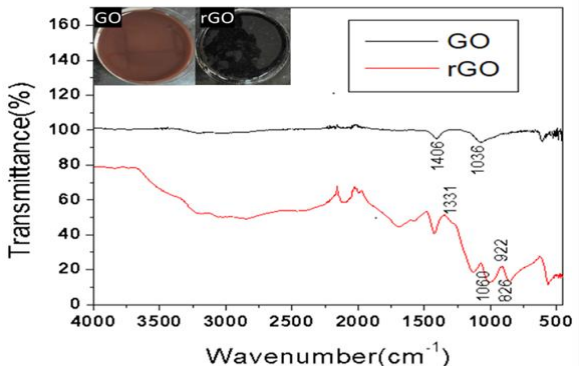

Figure 1 FT-IR spectra of Graphene Oxide (GO) and rGO

Additionally, the morphological information of the rGO is shown in the SEM image (Fig.2a), where the exfoliated graphene layers spread out over a few hundred nanometres. Additionally, Fig. 2b EDAX spectra of rGO and Fig.2c display the atomic percentage of various elements in rGO. The existence of sulphur and nitrogen peaks, which are ascribed to the presence of thiol and amine groups, is linked to the functionalisation with thiourea and mercaptoacetic acid (Fig. 2c).

Transmission electron microscopy (TEM) (Fig.3) validated the formation of multilayer sheets of rGO.

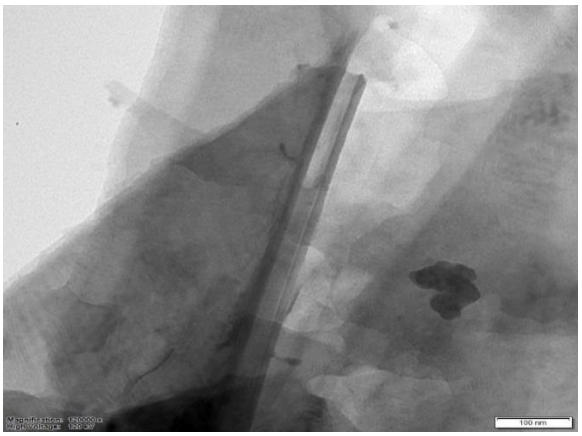

Figure 2 TEM image of rGO

Journal of Chemical Health Risks
www.jchr.org
JCHR (2025) 15(4), 662-669 | ISSN:2251-6727

The Raman Spectroscopy analysis (Fig. 4) depicts the presence of both characteristic D-band and G-band, indicating a graphene or graphite-like structure. For D-band lies at 1362 cm^{-1} and 1321 cm^{-1} for GO and rGO, respectively. Whereas the G-band was observed at 1599 cm^{-1} and 1592 cm^{-1} for GO and rGO, respectively. The D-band signifies the stretching vibrations of carbon with sp^3 hybridization and is associated with defects in the sample structure, specifically in the lattice of carbon. Whereas the G-band is attributed to the in-lane vibrations of the carbon atoms with sp^2 hybridization (Zrimsek et al., 2017). The I_D/I_G ratio indicates the degree of disorder. Here, the I_D/I_G ratio for GO and rGO is 1.95 and 0.92, respectively, clearly showcasing the more ordered structure of rGO due to the reduction in the number of functional groups as compared to GO (Jahan et al., 2022). The surface area of rGO is found to be 54.233 m^2/g. X-Ray Diffraction shows the rGO (Fig.5.) at 2θ=24.5°, which corresponds to the (002) plane, and a lesser peak at 2θ=43.088° for the (100) plane(Verma & Dutta, 2015).

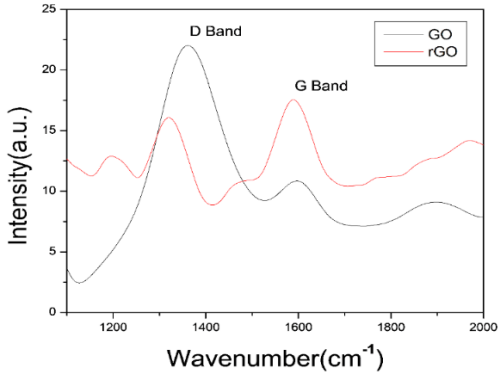

Figure 4 Raman spectra of GO and rGO showing the characteristic G and D bands

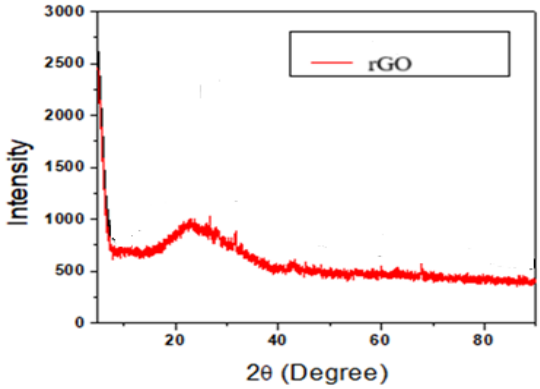

Figure 5 X-Ray diffraction pattern of rGO

3.2. Adsorption studies

3.2.1 Adsorption isotherms

Iron ion adsorption on rGO nanosheets was investigated employing the Freundlich, Langmuir, and Temkin adsorption isotherms at 298 K.

At equilibrium, the Fe^{2+} ion adsorption capacity (q_e) was calculated as follows:

$$q_e = \frac{C_o - C_e}{m} * V \qquad (1)$$

It is appropriate to use the Freundlich isotherm for heterogeneous surfaces and the linear form of the Freundlich isotherm is represented as follows:

$$\log q_e = \log K_F + \frac{1}{n} \log C_e \qquad (2)$$

where 1/n is connected to the heterogeneity parameter of the sorbent and signifies the strength of adsorption during the adsorption process, and K_F is the Freundlich isotherm constant (in mg g-1), which is an approximation of the adsorption capacity.

The linear fit of the plot of log q_e and log Ce ($R^2 = 0.577$) was used to establish the parameters K_F and n, which are distinctive of the sorbent-sorbate system. If n = 1, the number n indicates whether the adsorption process is independent of the sorbate concentration, or if cooperative adsorption (1/n > 1) is responsible for the process, or if normal adsorption (1/n <1).

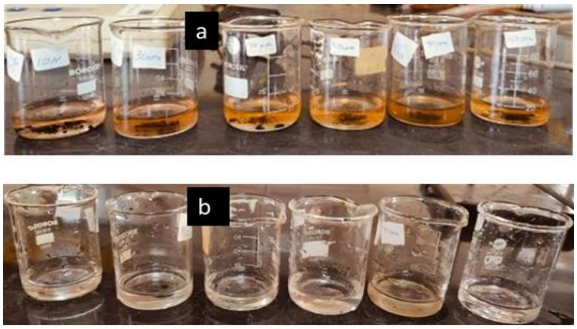

Figure 6 Solution containing rGO (a) Before Adsorption (b) after Adsorption of Fe^{2+} ion

The maximal monolayer coverage on the adsorbent surface was quantitatively described by the Langmuir adsorption isotherm model, which depicts the equilibrium distribution of metal ions between the solid and liquid phases. The adsorption data were analysed in light of this model. The model does not account for

Journal of Chemical Health Risks
www.jchr.org
JCHR (2025) 15(4), 662-669 | ISSN:2251-6727

adsorbate transmigration across the adsorbent surface; instead, it assumes that the adsorbent surface has a finite number of identical sites with uniform energies of adsorption onto the surface.

The linear form of the Langmuir adsorption isotherm is given as

$$\frac{C_e}{q_e} = \frac{1}{K_L q_{max}} + \frac{C_e}{q_{max}} \qquad (3)$$

And the equilibrium parameter is

$$R_L = \frac{1}{1+(1+k_L C_o)} \qquad (4)$$

The adsorption capacity and concentration of iron ions at equilibrium conditions are denoted by q_e (in mg g-1) and C_e (mg L^{-1}), respectively; the Langmuir isotherm constant (L mg^{-1}) is

Represented by k_L, the maximum adsorption capacity of the adsorbent (rGO) is denoted by q_{max} (mg g^{-1}), and the initial concentration of iron ions is denoted by Co. The separation factor, or R_L value, represents the kind of adsorption and is unfavourable if $R_L > 1$, irreversible if $R_L = 0$, linear if $R_L = 1$, and favourable if $0 < R_L < 1$. The plot of C_e/q_e vs. C_e's slope and intercept was used to calculate the values of q_{max} and k_L, respectively. The iron ion adsorption on GO @Thio was shown to favour the Langmuir model (R^2 = 0.994), which assumes monolayer adsorption in the absence of any chemical interaction between the sorbent and sorbate. The q_e is predicted from the Langmuir adsorption isotherm data to grow with temperature, and the adsorption capacity (K_F) also explains this behaviour.

Additional understanding of the adsorption process was acquired through research on the Temkin isotherm model, which postulates that adsorption results from chemical interactions and that, as a result of adsorbate–adsorbent interactions, the heat of adsorption reduces linearly rather than logarithmically with surface coverage. The Temkin model is defined as follows:

$$q_e = \frac{RT}{b} \ln k_T + \frac{RT}{b} \ln C_e \qquad (5)$$

where RT/ b = B, q_e and C_e are the same as defined earlier, R is the universal gas constant, b is the Temkin isotherm constant, B is the Temkin constant related to heat of adsorption (J mol^{-1}), k_T is the Temkin isotherm equilibrium constant (L g^{-1}). The other parameters of the Temkin model (Fig. 6b) are the same as previously defined. A linear fit (R^2 = 0.938) was obtained when plotting q_e against lnC_e, suggesting that iron ion adsorption on the adsorbent was in fairly good agreement with the Temkin model.

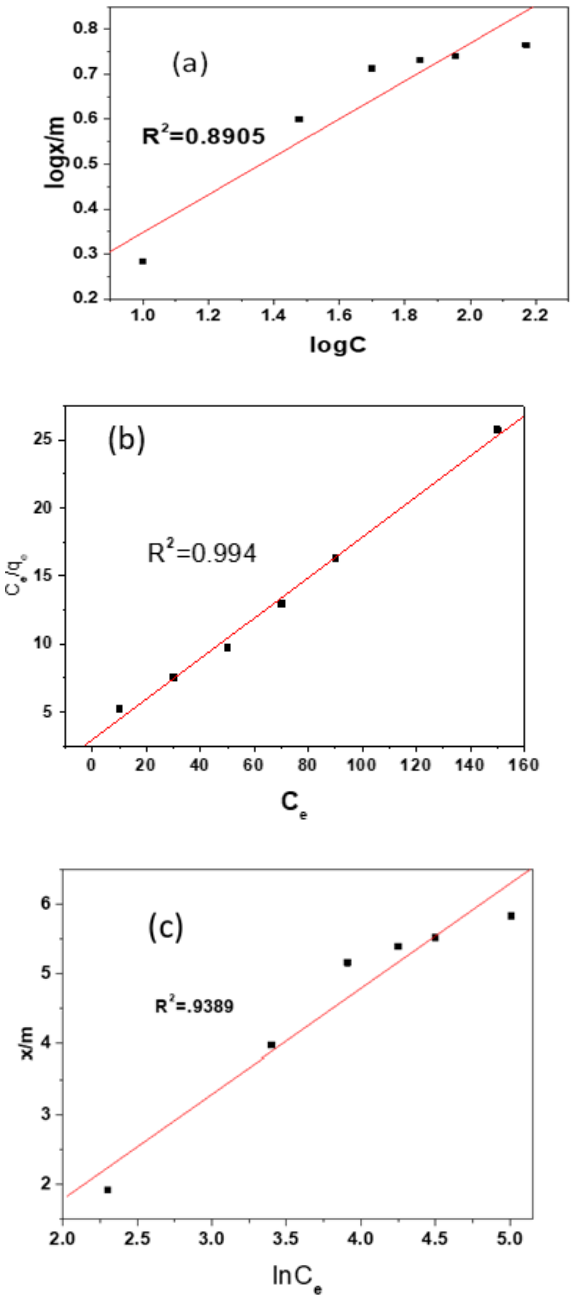

Figure 3 Adsorption of Fe2+ ions on rGO as modelled by (a) Freundlich adsorption isotherm, (b) Langmuir adsorption isotherm, (c) Temkin adsorption isotherm

Journal of Chemical Health Risks
www.jchr.org
JCHR (2025) 15(4), 662-669 | ISSN:2251-6727

Table 1 Parameters of various adsorption isotherms

Isotherm	Constant	R^2
Freundlich	2.084 mg/g	0.8905
Tempkin	0.444 L/g	0.9389
Langmuir	0.049 L/mg	0.994

3.2.2. Adsorption Kinetics

Adsorption is a physicochemical process in which the adsorbent is transferred from the solution phase to its surface. The adsorption process and reaction pathways are better understood thanks to the adsorption kinetics. Intraparticle diffusion, pseudo-first order, and pseudo-second order models provide the best explanations for the kinetic study, which also describes the solute absorption rates.(Ho & McKay, 1999) This is the pseudo-first order kinetics (Fig.7a) model's linear form represented as

$$\log(q_e - q_t) = \log q_e - \frac{k_1}{2.303} t \qquad (6)$$

Here, k_1 is the pseudo-first-order rate constant, while qe and qt stand for the adsorption capacities at equilibrium and at any given time t, respectively. As illustrated in (Fig.7b), the linear fit of the plot of $\log(q_e\text{-}q_t)$ vs. time (t) had a weak correlation (R^2 = 0.988). The adsorption of Fe^{2+}ions on rGO was presumably based on pseudo-first order (Ho & McKay, 1999). Hence, Diffusion-controlled adsorption resulted.

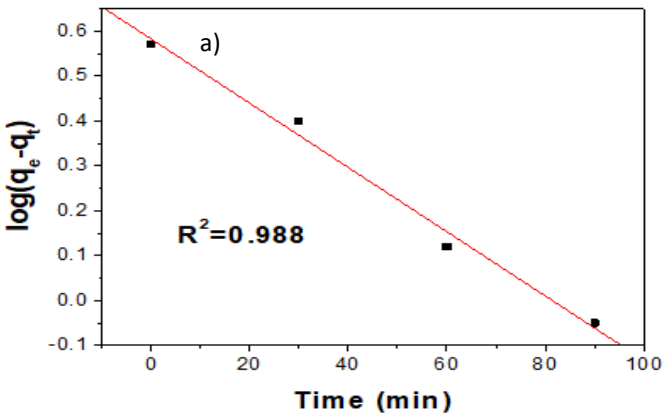

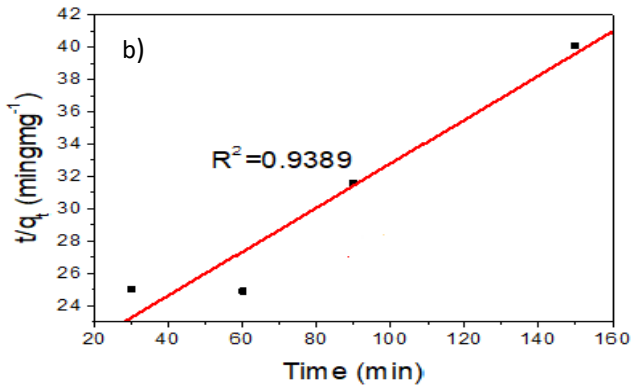

Figure 4 The adsorption of Fe2+ ions on rGO fitted with (a) pseudo first order kinetic model; (b) pseudo second order kinetic model

The pseudo second order kinetic model is expressed in linear form as follows:

$$\frac{t}{q_t} = \frac{1}{k_2 q_e{}^2} + \frac{1}{q_e} t \qquad (7)$$

Where q_e and q_t are the same as previously defined for the pseudo first order kinetics equation, k_2 is the second order rate constant. The t/q_t vs. t plot's linear fit indicated a correlation coefficient (R^2 = 0.9389), as seen in Fig.7b.This implied that the Fe^{2+} ion adsorption on GO does not adhere to the pseudo-second order model.

The kinetics models of pseudo-first and pseudo-second order strongly suggested that diffusion was the cause of the Fe^{2+} ion adsorption on rGO.

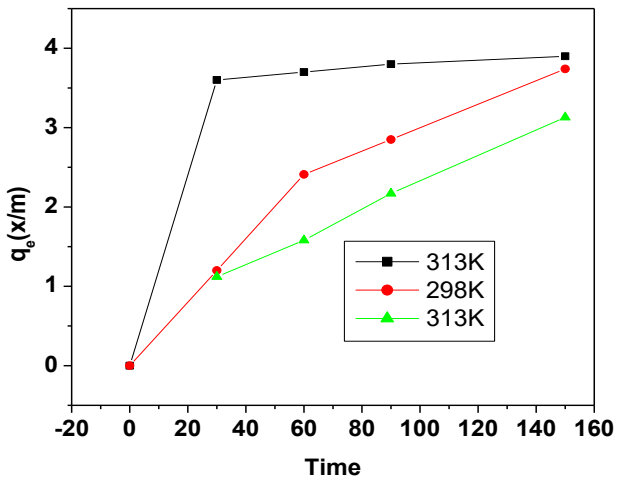

Figure 5 Effect of contact time and temperature on qe values of Fe^{2+} ion adsorption by rGO

Journal of Chemical Health Risks

www.jchr.org

JCHR (2025) 15(4), 662-669 | ISSN:2251-6727

3.2.3 Thermodynamic studies.

At three distinct temperatures, 273 K, 298 K, and 313 K, the impact of temperature on the adsorption of Fe^{2+} ions on rGO was investigated. The increase in qe value was observed with an increase in temperature, exhibiting an endothermic nature of the adsorption. Fig.8 indicates that adsorption is endothermic.

4. Conclusion

The effective production of modified graphene oxide (rGO) with specific functional groups for efficient adsorption of Fe^{2+} ions has been thoroughly investigated. Due to heterogeneous binding sites, the adsorption isotherm, kinetic, and thermodynamic studies revealed a dual process of chemisorption and physisorption following the pseudo-first-order kinetics. The percentage of adsorption is 89.69%. The dominance of monolayer adsorption is demonstrated by the Langmuir adsorption isotherm. The surface area of rGO is found to be 54.233 m^2/g.

References

1. Akaji, S. R., & Dewez, D. (2020a). Functionalized Glutathione on Chitosan-Genipin Cross-Linked Beads Used for the Removal of Trace Metals from Water. *International Journal of Biomaterials*, *2020*, 1–14. https://doi.org/10.1155/2020/4158086
2. Akaji, S. R., & Dewez, D. (2020b). Functionalized Glutathione on Chitosan-Genipin Cross-Linked Beads Used for the Removal of Trace Metals from Water. *International Journal of Biomaterials*, *2020*, e4158086. https://doi.org/10.1155/2020/4158086
3. Banazadeh, A., Mozaffari, S., & Osoli, B. (2015). Facile synthesis of cysteine functionalized magnetic graphene oxide nanosheets: Application in solid phase extraction of cadmium from environmental sample. *Journal of Environmental Chemical Engineering*, *3*(4), 2801–2808.
4. Gupta, V. K., Gupta, B., Rastogi, A., Agarwal, S., & Nayak, A. (2011). Pesticides removal from waste water by activated carbon prepared from waste rubber tire. *Water Research*, *45*(13), 4047–4055. https://doi.org/10.1016/j.watres.2011.05.016
5. Hamdouni, A., Montes-Hernandez, G., Tlili, M., Findling, N., Renard, F., & Putnis, C. V. (2016). Removal of Fe(II) from groundwater via aqueous portlandite carbonation and calcite-solution interactions. *Chemical Engineering Journal*, *283*, 404–411. https://doi.org/10.1016/j.cej.2015.07.077
6. Ho, Y.-S., & McKay, G. (1999). Pseudo-second order model for sorption processes. *Process Biochemistry*, *34*(5), 451–465.
7. Hong, Y.-S., Song, K.-H., & Chung, J.-Y. (2014). Health Effects of Chronic Arsenic Exposure. *Journal of Preventive Medicine and Public Health*, *47*(5), 245–252. https://doi.org/10.3961/jpmph.14.035
8. Huang, D., Li, B., Wu, M., Kuga, S., & Huang, Y. (2018). Graphene Oxide-Based Fe–Mg (Hydr)oxide Nanocomposite as Heavy Metals Adsorbent. *Journal of Chemical & Engineering Data*, *63*(6), 2097–2105. https://doi.org/10.1021/acs.jced.8b00100
9. Jahan, N., Roy, H., Reaz, A. H., Arshi, S., Rahman, E., Firoz, S. H., & Islam, Md. S. (2022). A comparative study on sorption behavior of graphene oxide and reduced graphene oxide towards methylene blue. *Case Studies in Chemical and Environmental Engineering*, *6*, 100239. https://doi.org/10.1016/j.cscee.2022.100239
10. Khorshidi, P., Shirazi, R. H. S. M., Miralinaghi, M., Moniri, E., & Saadi, S. (2020). Adsorptive removal of mercury (II), copper (II), and lead (II) ions from aqueous solutions using glutathione-functionalized NiFe2O4/graphene oxide composite. *Research on Chemical Intermediates*, *46*(7), 3607–3627. https://doi.org/10.1007/s11164-020-04164-1
11. Kumar, A. S. K., & Jiang, S.-J. (2015). Preparation and characterization of exfoliated graphene oxide–L-cystine as an effective adsorbent of Hg (II) adsorption. *RSC Advances*, *5*(9), 6294–6304.
12. Li, Z., Chen, F., Yuan, L., Liu, Y., Zhao, Y., Chai, Z., & Shi, W. (2012). Uranium (VI) adsorption on graphene oxide nanosheets from

aqueous solutions. *Chemical Engineering Journal*, *210*, 539–546.

13. Mirnezami, S. Y., Davallo, M., Sohrabi, M., Motiee, F., & Khosravi, M. (2019). Synthesis of magnetic graphene/nylon 6 nanocomposite and its application for removal of lead ions from aqueous solutions: Isotherm and kinetic studies. *Research on Chemical Intermediates*, *45*(11), 5519–5533. https://doi.org/10.1007/s11164-019-03917-x
14. Patel, M., Bisht, N., Prabhakar, P., Sen, R. K., Kumar, P., Dwivedi, N., Ashiq, M., Mondal, D. P., Srivastava, A. K., & Dhand, C. (2023). Ternary nanocomposite-based smart sensor: Reduced graphene oxide/polydopamine/alanine nanocomposite for simultaneous electrochemical detection of Cd2+, Pb2+, Fe2+, and Cu2+ ions. *Environmental Research*, *221*, 115317. https://doi.org/10.1016/j.envres.2023.115317
15. Ratnam, M. V., Akilamudhan, P., Kumar, K. S., Reddy, S. N., Rao, K. N., Shaik, F., Prasad, D. M. R., & Rangabhashiyam, S. (2023). Carbon-Based Nanoadsorbents for the Removal of Emerging Pollutants. *Adsorption Science & Technology*, *2023*, 3579165. https://doi.org/10.1155/2023/3579165
16. Rizzo, C., Andrews, J. L., Steed, J. W., & D'Anna, F. (2019). Carbohydrate-supramolecular gels: Adsorbents for chromium (VI) removal from wastewater. *Journal of Colloid and Interface Science*, *548*, 184–196.
17. Seenivasan, R., Chang, W.-J., & Gunasekaran, S. (2015). Highly Sensitive Detection and Removal of Lead Ions in Water Using Cysteine-Functionalized Graphene Oxide/Polypyrrole Nanocomposite Film Electrode. *ACS Applied Materials & Interfaces*, *7*(29), 15935–15943. https://doi.org/10.1021/acsami.5b03904
18. Sherlala, A. I. A., Raman, A. A. A., Bello, M. M., & Asghar, A. (2018). A review of the applications of organo-functionalized magnetic graphene oxide nanocomposites for heavy metal adsorption. *Chemosphere*, *193*, 1004–1017. https://doi.org/10.1016/j.chemosphere.2017.11.093
19. Verma, S., & Dutta, R. K. (2015). A facile method of synthesizing ammonia modified graphene oxide for efficient removal of uranyl ions from aqueous medium. *RSC Advances*, *5*(94), 77192–77203. https://doi.org/10.1039/C5RA10555B